Emitters of N-photon bundles
Supplementary Information

C. Sánchez Muñoz,[1] E. del Valle,[1] A. González Tudela,[2] K. Müller,[3]
S. Lichtmannecker,[3] M. Kaniber,[3] C. Tejedor,[1] J.J. Finley,[3] and F.P. Laussy[1]

[1] *Condensed Matter Physics Center (IFIMAC), Departamento de Física Teórica de la Materia Condensada, Universidad Autónoma de Madrid, 28049 Madrid, Spain*
[2] *Max-Planck-Institut für Quantenoptik, Hans-Kopfermann-Str. 1, 85748 Garching, Germany*
[3] *Walter Schottky Institut, Technische Universität München, Am Coulombwall 4, 85748 Garching, Germany*

I. GIANT RABI OSCILLATIONS BETWEEN ARBITRARILY DISTANT MANIFOLDS.

Without dissipation, the coherent driving at low intensity of the detuned cQED system probes the Jaynes–Cummings resonances. This leads to giant Rabi oscillations between the vacuum state $|0\mathrm{g}\rangle$ on the one hand and the quantum emitter (QE)'s excited state with N photons in the cavity $|N\mathrm{e}\rangle$, on the other hand. Since N can be any integer, depending on which resonance is driven, the superposition is between states that differ arbitrarily in energy:

$$|\psi_N\rangle = \frac{1}{\sqrt{2}}\left(|0\mathrm{g}\rangle + |N\mathrm{e}\rangle\right) . \tag{1}$$

Such a superposition has been hypothetically referred to describe "spooky" features of quantum mechanics, like non-conservation of energy (the collapse of such a wavefunction suddenly realizes a state that has either no energy or the huge amount $\hbar\omega_\sigma + N\hbar\omega_a$) [1, 2]. We provide here a mechanism to actually realize it.

The ease in setting up the state Eq. (1), that would require extremely difficult operations with little chances of success with a direct engineering [3], is to be atoned by the timescales involved. The Rabi oscillations become vanishingly slow for increasing differences of energy. In what follows, we derive analytical expressions for their frequencies.

In the rotating frame of the laser, the Hamiltonian becomes $H = \delta_a a^\dagger a + \delta_\sigma \sigma^\dagger\sigma + g(a^\dagger\sigma + \sigma^\dagger a) + \Omega(\sigma^\dagger + \sigma)$ and we are left with solving Schrödinger equation $|\dot{\psi}\rangle = -iH|\psi\rangle$, whose formal solution in the basis of the eigenstates $|\phi_i\rangle$ of H reads:

$$|\psi(t)\rangle = c_1|\phi_1\rangle e^{-iE_1 t} + c_2|\phi_2\rangle e^{-iE_2 t} + \cdots \tag{2}$$

with the coefficients $c_i = \langle\phi_i|\psi_0\rangle$ to be determined by the initial state $|\psi_0\rangle$. Using the basis of bare states, $\{|0\rangle, |1\rangle, |2\rangle, |3\rangle, \ldots\} \equiv \{|0\mathrm{g}\rangle, |0\mathrm{e}\rangle, |1\mathrm{g}\rangle, |1\mathrm{e}\rangle, \ldots\}$, one can represent the wavefunction through the probabilities p_i for the system to be in the state $|i\rangle$:

$$p_i(t) = |\langle i|\psi(t)\rangle|^2 = \sum_{j,k} c_j c_k^* \langle i|\phi_j\rangle\langle\phi_k|i\rangle e^{i(E_k - E_j)t} . \tag{3}$$

While in general, to first approximation, the system remains trivially in the ground state, one finds that for certain frequencies of excitation, ω_N, there is a striking change to full-magnitude Rabi oscillations, with $p_{0g} = p_{Ne} = 1/2$ and all other $p_k = 0$. This is the case whenever the laser hits a $(N+1)$-photon resonance of the Jaynes–Cummings ladder, as explained in the main text. In the purely Hamiltonian picture, such resonances can be revealed by plotting the amplitude of the Rabi oscillations, that is, their time average which is given by the sum of the non-oscillating terms in Eq. (3), i.e., $\langle p_i\rangle = \sum_j |c_j|^2 |\langle i|\phi_j\rangle|^2$. These are displayed in Fig. S1 and are in direct correspondence with the resonances in $g^{(n)}$ shown in Fig. 3c of the text. This implies that this giant Rabi dynamics of distant manifolds is responsible for the strong N-photon correlations in the detected field when opening the dissipative channel. One can see neatly how the laser "strikes different quantum chords" and brings in resonance the vacuum (upper red curve) with each one of the manifolds in succession, climbing the Jaynes–Cumming ladder in the process. There is a neat transition from the quantized nature of the cavity QED system on the QE side, on the right of the Fig. S1a, towards a continuum as it bridges to the classical field of the cavity, on the left. Note that the resonances widths decay exponentially with the number of photons in the superposition and

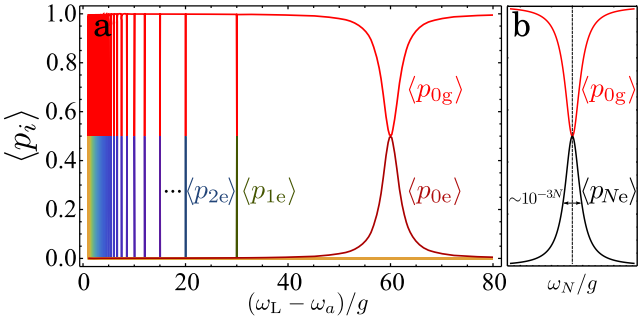

FIG. S1: **a**, Probability of occupation of the states $\{|0\mathrm{g}\rangle, |0\mathrm{e}\rangle, |1\mathrm{g}\rangle, \ldots\}$ as a function of the excitation frequency. This shows how the laser can "strike" quantum resonances to trigger full-amplitude Rabi oscillations between the vacuum $|0\mathrm{g}\rangle$, in red, and any of the excited states $|N\mathrm{e}\rangle$. The multi-photon resonances of states with N photons in the cavity have a width of the order of 10^{-3N}. They thus appear as straight vertical lines on the scale of panel a. A magnification of a generic resonance is shown in **b**.

are thus extremely sharp, appearing like δ functions in the plot. A magnification of a generic resonance is provided in Fig. S1b.

Such strong resonances suggest a change in the structure of the energy levels induced by the laser, which result, at certain frequencies, in the isolation of the two states involved in the N-polariton state (1). A convenient way to study analytically such an emerging manifold structure is to resort to the Hamiltonian H in the rotating frame of the laser in the limit $\Omega \to 0$. The information of how the states are coupled when the laser is switched on is encoded in the eigenenergies $E^n_\pm - n\omega_\mathrm{L}$ now explicitely dependent on the laser frequency. All the resonances occur when two eigenenergies cross, yielding the resonant frequencies:

$$\omega^{n,\xi}_{n',\xi'} = \omega_a + \frac{\xi\sqrt{ng^2+\Delta^2/4} - \xi'\sqrt{n'g^2+\Delta^2/4}}{n-n'}\,, \quad (4)$$

with n, $n' \in \mathbf{N}$ (and $n \neq n'$) and ξ, $\xi' \in \{-1, 1\}$ corresponding to lower and upper polaritons, respectively. The ground state is given by $\xi = -1$, $n = 0$. This predicts more resonances than those plotted in Fig. S1, that appear as satellite peaks to the main resonances which are $\omega_N = \omega^{N+1,1}_{0,-1}$. The additional resonances are indeed observed when zooming in on the appropriate range. They are small as they do not realize full-amplitude Rabi oscillations, and correspond to n-photon transitions between two manifolds not involving the ground state. These peaks would yield full Rabi oscillations if the initial state would be chosen adequately.

Since an isolated manifold emerges at each resonance, whose dynamics can be well separated from the rest of the states, we can perform an adiabatic elimination to retain only the coupling between the relevant states and derive an effective Hamiltonian that provides the Rabi frequencies. We will treat the case of $|\psi_2\rangle$ explicitly. In that situation, it is enough to restrict ourselves up to the second manifold, and use for the solution the ansatz $|\psi(t)\rangle = \sum_{i=0}^{4} c_i(t)|i\rangle$. The Schrödinger equation for the coefficients reads:

$$i\begin{pmatrix}\dot{c_1}\\ \dot{c_2}\\ \dot{c_3}\\ \dot{c_4}\\ \dot{c_5}\end{pmatrix} = \begin{pmatrix}0 & \Omega & 0 & 0 & 0\\ \Omega & \delta\sigma & g & 0 & 0\\ 0 & g & \delta_a & \Omega & 0\\ 0 & 0 & \Omega & \delta_\sigma+\delta_a & \sqrt{2}g\\ 0 & 0 & 0 & \sqrt{2}g & 2\delta_a\end{pmatrix}\begin{pmatrix}c_1\\ c_2\\ c_3\\ c_4\\ c_5\end{pmatrix}\,.$$

Setting $\dot{c_1} = \dot{c_2} = \dot{c_4} = 0$, one can eliminate c_1, c_2 and c_4 from the system of differential equations, and get the corresponding effective Hamiltonian:

$$H_\mathrm{eff} = \begin{pmatrix} \frac{\Omega^2}{\delta_\sigma(1-g^2/(\delta_a\delta_\sigma))} & \frac{g\Omega^2}{\delta_a\delta_\sigma}\left(\frac{1}{1-g^2/(\delta_a\delta_\sigma))}\right) \\ \frac{g\Omega^2}{\delta_a\delta_\sigma}\left(\frac{1}{1-g^2/(\delta_a\delta_\sigma))}\right) & \delta_a+\delta_\sigma-\frac{g^2}{\delta_a}+\left(\frac{1}{1-g^2/(\delta_a\delta_\sigma))}\right)\frac{\Omega^2}{\delta_a}\end{pmatrix}\,. \quad (5)$$

The Rabi frequency for the two photon resonance is thus obtained as:

$$\Omega^{(2)}_\mathrm{eff} = \frac{g\Omega^2}{\delta_a\delta_\sigma - g^2}\,. \quad (6)$$

If $\delta_a, \delta_\sigma \gg g, \Omega$, the Rabi frequency takes the form $(\sqrt{g}\Omega)^2/(\delta_a\delta_\sigma)$ of a generalized Lamb shift for the Jaynes–Cummings model, that is, it shows the energy shift of the coupled light-matter system by the driving laser as opposed to the conventional scenario where the light mode shifts the QE alone.

Following the same procedure for the next manifolds of excitation, the Rabi frequency up to any order can be obtained analytically as:

$$\Omega^{(n)}_\mathrm{eff} = \frac{g^{n-1}\Omega^n\sqrt{(n-1)!}}{D_{2(n-1)}}\,, \quad (7)$$

where D_n is defined through the recurrence relation $D_n = a_n D_{n-1} - b_n^2 D_{n-2}$ with $D_0 = 1$, $D_1 = a_1$ with:

$$a_n = \begin{cases}\delta_\sigma + \frac{n-1}{2}\delta_a\,, \\ \frac{n}{2}\delta_a\,,\end{cases} \quad b_n = \begin{cases}-\Omega\,, & n \text{ odd}\\ \sqrt{\frac{n}{2}}g\,, & n \text{ even}\end{cases}$$

resulting in exact expressions easily obtained but too heavy to write here. Approximated versions in the limit of large detunings are much simpler, such as the Rabi frequency for $|\psi_3\rangle$:

$$\Omega^{(3)}_\mathrm{eff} \approx \frac{g^2\Omega^3}{\sqrt{2}(\delta_a^3\delta_\sigma + \delta_a^2\delta_\sigma^2)}\,. \quad (8)$$

This completes the characterization of the remarkable states of Eq. (1). The quantum superposition between the vacuum and a highly excited state is possible, although it involves very sharp resonances with slow Rabi oscillations. We proceed to the case where such resonances can be brought to immediate use for actual devices, thanks to dissipation.

II. TRANSITION FROM THE JAYNES–CUMMINGS DYNAMICS TO THE MOLLOW DYNAMICS.

The Hamiltonian used in this work covers fully and bridges between two pillars of quantum nonlinear optics, namely, the Jaynes–Cummings model on the one hand and the Mollow physics of the dressed atom on

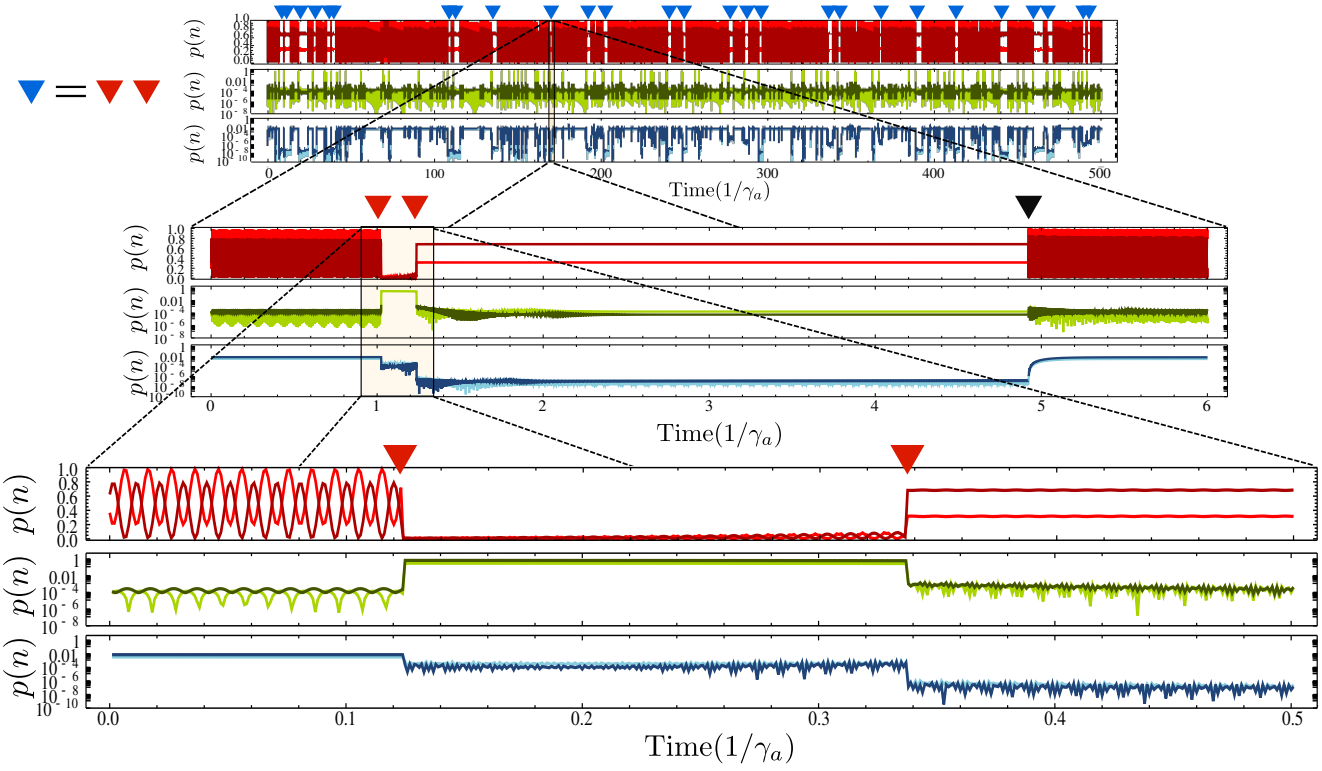

FIG. S2: (Colour online) Quantum trajectory showing the different timescales involved in the mechanism of two-photon emission. The colour code and notations are the same as Fig. 4a–c of the text. Top: long time-range dynamics. Two-photon events are identified as blue triangles while the underlying single-photons are identified as red triangles. Emission from the QE is shown as a black triangle. Statistics of these events are given by the two-photon second order correlation function $g_2^{(2)}(\tau)$. Medium: White stripes are due to the absence of Rabi flopping of the QE after the second cavity emission, and its length is given by the QE lifetime. After a subsequent QE emission, the Rabi flopping is restored and the construction of a new two-photon state in the cavity is resumed. This manifests as a dependence of the statistics of the two-photon bundles on the QE lifetime (Fig. S6a). Bottom: The shortest timescale on the dynamics is given by the Mollow frequency, that precedes the sequence of rapid two photons emission.

the other hand. The transition is rich and complicated and this work certainly does not exaust it. It is maybe better comprehended by following the resonances themselves, as the laser intensity is tuned up. This is shown in Fig. 3a of the text for three pumping values and is provided for all pumpings in the movie `JCMollowTransition.mp4`. The system starts at low pumping intensity with resonances at ω_N [cf. Eq. (1) from the text]. Each resonance corresponds to a giant Rabi oscillations described by Eq. (1). In this regime, the resonances in $g^{(n)}$ at various $\omega_{\rm L}$ (shown in the animation for $n = 2$) change magnitude relatively to each other with increasing pumping but stay pinned to the Jaynes–Cumming ladder. At some point, the laser takes over the cavity, resulting in a blueshift of the resonances due to state dressing. This is the transition to the Mollow regime. At large pumping, the cavity that was previously constituting half of the system along with the QE, becomes a mere Purcell enhancer of the dynamics, now dominated by the laser that is driving the QE. Note that the QE always remains the central actor: the quantum character of the emission comes from the QE, while the cavity, or the laser, are classical probes or catalysts, that trigger, store and convey the engineered emission from the active material [4].

The transition is also pictured from an alternative point of view in Fig. 4a–c, through the probabilities derived from the wavefunction. The Jaynes–Cummings limit, Fig. 4a, is simply the superposition of two states. The Mollow limit, Fig. 4b, exhibits a more complicated dynamics that involves a fast Rabi flopping of the dot and starts to mix more states from various manifolds, but still keeping the feature of involving only a few of them. The same limit with dissipation, Fig. 4c, is the case that realizes N-photon emission. The excitation of the multi-photon resonances in this case brings in succession various regimes that evolve with different timescales, and between which the system transits by collapse of the wavefunction. This is shown in Fig. S2, that displays a long portion of one quantum trajectory (top) that is expanded successively for regions of interest (from top to bottom). The top panel depicts the bundle emission, indicated by blue triangles, at the timescale of detection. This appears as white stripes in an otherwise fast oscillating dynamics. Zooming in on such a stripe, second row, one see that the bundle

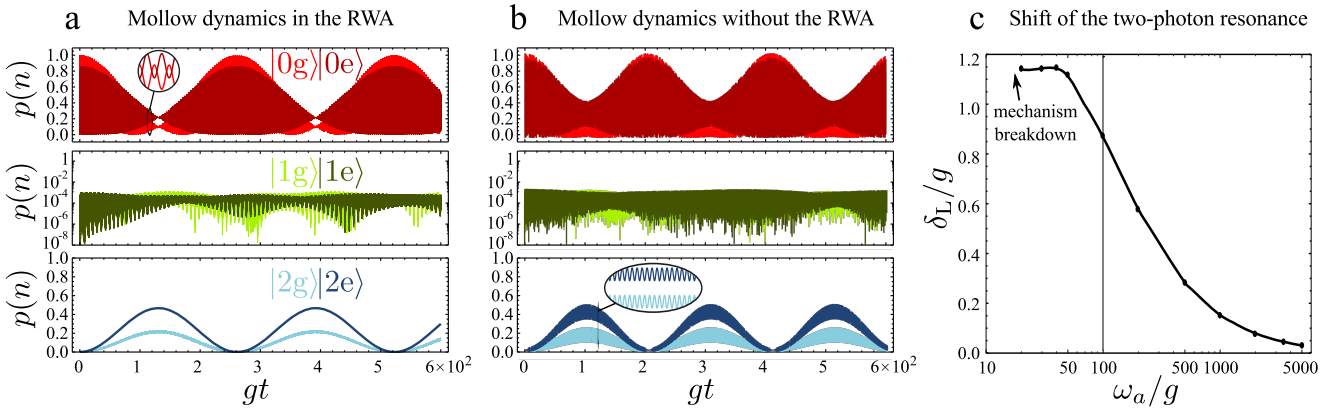

FIG. S3: **a**, Dynamics of the strongly-driven and largely detuned system within the RWA (panel b of Fig. 4 in the main text). **b**, The corresponding dynamics without the RWA in the USC regime for $\omega_a/g = 100$. While the counter-rotating terms have an observable difference (starting with ratio $\omega_a/g \lesssim 2000$), the phenomenology remains essentially the same. **c**, Shift δ_L of the laser frequency ω_L to trigger the two-photon resonance, caused by the counter-rotating terms in the Mollow regime of strong driving. At about $\omega_a/g \approx 20$, the mechanism breaks down and fails to produce a two-photon resonance with large amplitude Rabi oscillations. This is the regime where the RWA fails completely.

is composed of two single-photons, depicted as red triangles. This window contains the two-photon emission iself, on a short timescale, followed by the reloading time, ruled by the QE. This determines the statistics of bundle emission. Finally, zooming in on the two-photon emission itself, last row, one can resolve the characteristic time of the two-photon emission process, given by the cavity lifetime. The shortest timescale is that of the Mollow Rabi floping, which governs the dynamics most of the time, and whose jolting by the quantum collapse provokes an avalanche of two-photon emission.

III. VALIDITY OF THE ROTATING WAVE APPROXIMATION.

The Jaynes–Cummings description is a simplified model which, despite its various approximations, has proved extremely successful in describing a large body of experiments which belong to the paradigm of a two-level system interacting with an harmonic mode [5]. The model can be subsequently extended and upgraded with features to account for more realistic situations, such as multiple-modes or many-body correlations [6–8] (see also Section VI that includes in this way effects of noise and decoherence), but the core of our effect can be tracked down to the Jaynes–Cummings physics itself.

One of the fundamental approximations that is performed at a very early stage of the model is the so-called Rotating Wave Approximation (RWA) [9], that neglects the counter-rotating terms of the light-matter interaction of the type $a\sigma$ and $a^\dagger\sigma^\dagger$, rapidly oscillating, as compared to the terms $a\sigma^\dagger$ and $a^\dagger\sigma$, which balance the frequencies of the modes at resonance. The approximation can lead to deviation from the actual result when the system is extremely far from resonance and/or when the frequency of the free oscillators is comparable to the exchange rate of excitation (coupling strength), in which case the system enters the regime of Ultra Strong Coupling (USC) [10, 11]. The RWA may also be an issue in the dynamics of the strongly driven two-level system alone, where deviations from the approximation manifest as the Bloch-Siegert shift [12]. Since our system invokes both strong driving of the QE on the one hand and detuning on the other hand, we must consider the validity and effect of the RWA.

The validity of the RWA for the strongly driven Jaynes–Cummings model has been studied in the literature [13, 14]. The counter-rotating terms were found to be important in the USC regime, for ratios of ω_a/g of order at least 10. For the three platforms of choice that we consider for our effect, one deals with ratios of typically several hundreds for superconducting qubits in a microwave resonator [15, 16], tens of thousands and above for quantum dots in microcavities [17] and millions and above for atoms [18]. For quantum dots and atoms, we are extremely far from the USC and the counter-rotating terms can be safely ignored. Superconducting qubits are closer to the regime where these term could matter, being indeed systems of choice to approach the USC regime with the possibility to get to the regime where the RWA breaks down completely [10]. To investigate the relevance of our system also for these systems sensitive to the RWA, we have performed numerical calculations that simultaneously take into account the counter-rotating terms for both the detuned QE-cavity coupling on the one hand and the driven QE on the other hand. We show in Fig. S3 the regime where the approximation is the less accurate, that is, at high driving intensity for a superconducting qubit situation where $\omega_g/g = 100$ (the deviation starts to be unnoticeable for values of

$\omega_a/g \gtrsim 2000$). The dynamics with RWA, which is the case of the text, is compared to that without the approximation. While the counter-rotating terms do affect the result, the effect is surprisingly resilient and retains its qualitative features. Indeed, the non-RWA dynamics mainly consists in a superimposition of very fast oscillations on top of the RWA dynamics, leading to a mere broadening of the oscillations. There is also a small renormalization of the frequencies, that is due to the shift of the resonance itself, shown in Fig. S3c. It takes counter-rotating terms of the order of a fraction of the detuning itself to completely spoil the effect and reach a dynamics that differs in essential terms from that of the RWA. This suggests that our scheme could be usefully transported till far into the USC regime where it could set the arena for interesting physics. Note that the problem of a proper theoretical model to describe the dissipative regime of an USC cavity QED setup is still open to debate [11, 19, 20] and the theoretical analysis of the output of such a device is thus way beyond the scope of this Supplementary Information.

IV. THE RELATION OF THE "BUNDLE" TO A FOCK STATE.

There are differences between the concept of a N-photon Fock state $|N\rangle$ and a bundle, as discussed in the main text. A Fock state $|N\rangle$ is a well defined object that does not account for any internal degree of freedom, while the bundle is the result of a dynamical process and henceforth it has an intrinsic temporal structure. This stems from the radiative cascade that gives rise to the emission of a bundle, which is clearly manifested as blocks emerging in the diagonal of the density matrix (see Fig. 5b). When the intracavity dynamics is dominated by this cascade events (as is the case in the regime of pure N-photon emission), the steady state probability of finding n photons inside the cavity is given by $p(n) = n_a/(Nn)$, cf. Eq. (5) in the text. In good approximation, $p(0) = 1 - \sum_{i=1}^{N} p(n)$ since probabilities for higher n are much smaller than those of the vacuum and the cascade of the bundle emission. Note that n_a/N is the bundle population. This probability is the result of a time-averaging over all cycles of the dynamics and is thus the one encoded in the diagonal element of the cavity density matrix, which is easily obtained from the master equation. The equation predicts a line in the graph of $p(n)$ when plotted as a function of $1/n$, as shown in Fig. S4a, rather than the peaked Kronecker distribution for a Fock state. The slope of the line corresponds to the bundle population n_a/N and its length to the number of photons in the bundle. Deviations from a straight line indicate a purity lower than 100%.

As mentioned in the main text, these internal correlations have a signature in the different time intervals that separate the photons if they are individually detected. The time separation between the photons composing a bundle is sketched in Fig. 5c in the main

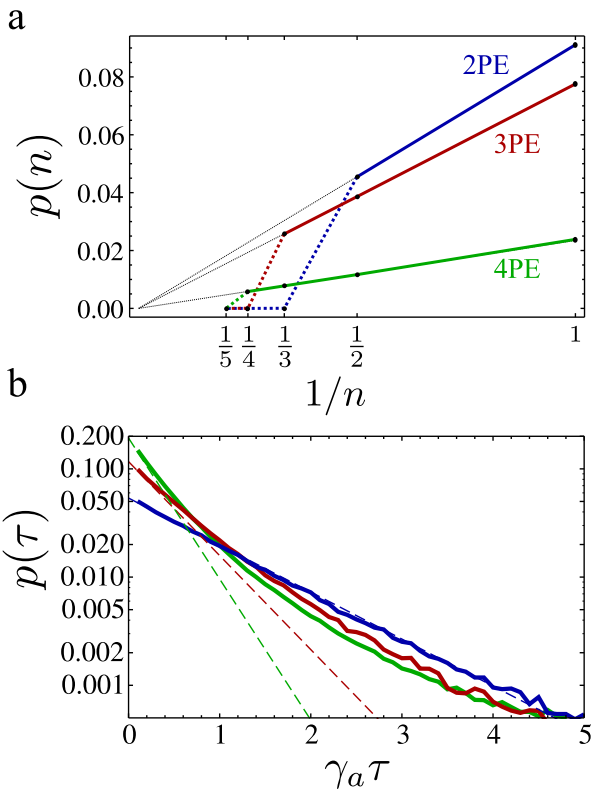

FIG. S4: (Colour online) Signatures of the internal structure of the N-photon bundles **a**, Diagonal elements of the cavity density matrix $p(n) = \langle n|\rho|n\rangle$ in the regimes from two to four-photon emission. Plotted as function of $1/n$, and according to Eq. (5) of the text, this yields a line in the regime of 100% purity with a slope equal to the bundle population n_a/N and extent equal to the number N of photons per bundle. **b**, Distribution of time intervals τ between successive photons of a bundler, in the regimes of two (blue), three (red) and four (green) photon emission. The distributions are $(N-1)$-exponential for N-photon emission, i.e., exponential for $N = 2$, bi-exponential for $N = 3$, etc. This confirms the time-distribution of the photons within the bundles as sketched in Fig. 5c in the main text. Thin lines show the $\exp(-(N-1)\tau)$ decay, to which the distributions get parallel to. The distribution of four-photon emission (green), for instance, gets parallel to all three lines in successive intervals.

text. This structure can be seen from the collected Monte-Carlo events by plotting the probability distribution of the detection of two successive photons with a given time difference, as is done in Fig. S4b, that shows a N-exponential decay for the cases of $2 \leq N \leq 4$-photon emission. One observes that the jitter imposes its largest toll for the case $N = 2$, since a bundler of N-photon is wrapped up in a time window of H_N/γ_a only (H_N is the Nth harmonic number, e.g., the overall lifetime is $\approx 2.28/\gamma_a$ for a bundle of five photons and is still smaller than $3/\gamma_a$ for a fat bundle of ten photons).

One can characterize alternatively the quantum state of the cavity field alone by turning to the Wigner distribution, which provides a self-contained and insightful

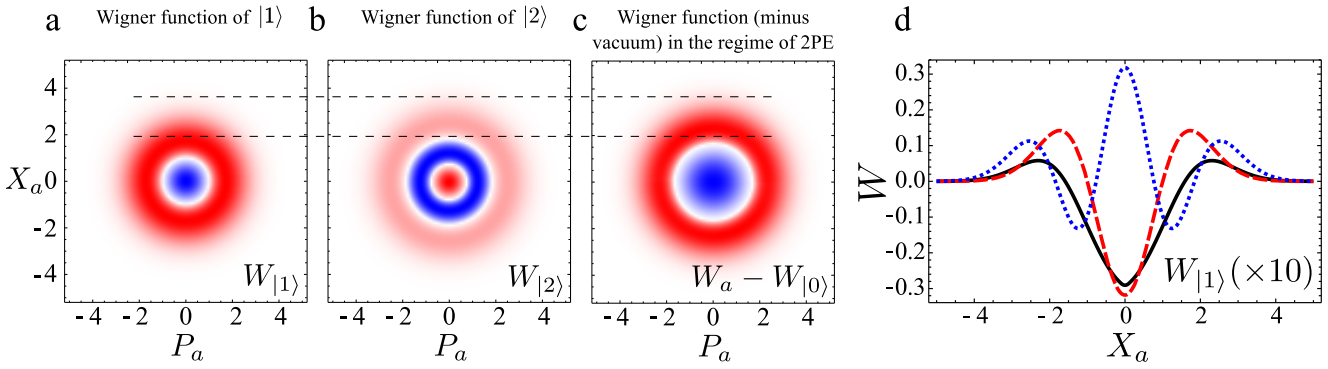

FIG. S5: (Colour online) Quantum state of the N–photon emitter. **a–c**, Wigner representation of the cavity field, comparing the Wigner distribution of the Fock states $|1\rangle$ (a) and $|2\rangle$ (b) with that of the cavity field in the regime of two-photon emission, to which we removed the predominant Wigner function of the vacuum. As also seen in the cut along a radius in **d**, the Wigner function of the two-photon emitter (solid black) is qualitatively similar to the Fock state $|1\rangle$ (dashed red) but with some attributes of Fock state $|2\rangle$ (dotted blue).

phase-space representation in the complex plane $\alpha = (X + iP)/2$ with X and P the quadratures [21]. The Wigner representation for the Fock projector $|m\rangle\langle n|$ is:

$$W_{mn}(r,\phi) = \frac{(-1)^n}{\pi}\sqrt{\frac{n!}{m!}}e^{i\phi(m-n)}r^{m-n}L_n^{m-n}r^2e^{-\frac{r^2}{2}}\,, \tag{9}$$

with $m \geq n$ ($W_{nm} = W^*_{mn}$) and $L_n^{m-n}(r^2)$ Laguerre polynomials. The Wigner function for the reduced density matrix $\rho = \sum_{mn}\rho_{mn}|m\rangle\langle n|$ is then $W = \sum_{mn}\rho_{mn}W_{mn}$. From this expression, one sees that the Wigner function of the Fock state $|N\rangle$ is described essentially by the Laguerre polynomials $\frac{(-1)^n}{\pi}L_n^0(r^2)e^{-r^2/2}$. Since $L_n^0(r^2)$ has $2n$ roots, the largest one of which being $\propto\sqrt{n}$, the associated Wigner function features $2n$-nodes contained in an annulus of mean radius $\sqrt{n}$, cf. Fig. S5a–b. The Wigner representation of the cavity field in our case features again predominantly the vacuum, given the underlying mechanism. By removing this vacuum so as to magnify the small structure due to the N-photon emission, one sees that the result resembles a Fock state $|1\rangle$, with the same number of nodes as its Wigner function, but with a size comparable to that of the Fock state $|2\rangle$, as shown in Fig. S5(a–c). We have checked that the same pattern holds for higher regimes of N-photon emission, namely, one-node circularly symmetric Wigner function with a radius that grows like the square root of N. This indicates the peculiar character of the state that gives rise to the bundle emission, mixing both attributes of, and departure from, the Fock state itself. The symmetric Wigner distribution is achieved in the regime of N-photon emission, with features mainly given by the diagonal elements of the cavity density matrix, Eq. (5) in the main text. It is surrounded by states with an intricate structure when not in the regime of 100% purity, as seen in the supplementary video `BundleQuantumState.mp4`.

Now that we have shown that our emitter produces states which are not strictly Fock states, we must balance the discussion by showing that there remains a deep connection with this concept. It is maybe best illustrated with the form of the generalized correlation function $g_N^{(n)}$, Eq. (6) of the text. While the term a^N appears nowhere explicitly in the Hamiltonian or any other part of the dynamics, it enters the correlation function that describes the statistics of emission and a in isolation plays no role by itself. Now, $(a^N)^\dagger$ is precisely the operator that creates a Fock state from the vacuum:

$$|N\rangle = \frac{(a^N)^\dagger}{\sqrt{N!}}|0\rangle\,. \tag{10}$$

The statistics of the bundles is therefore described by a quantity where the photon operator itself does not enter but needs to be upgraded to a Fock state creation operator. This demonstrates that there is a strong connection between a bundle and a Fock state of N photons. Surprisingly, while we could expect that a correlation function built on a^N operators would break for correlation times smaller than the coherence time of the bundle, that is, for $\tau \ll 1/\gamma_a$, the agreement remains perfect down to $\tau = 0$ coincidences. This suggests that regardless of the internal structure of the bundle, it is perceived as a Fock state in a measurement integrated over a small time window, or simply because of the time uncertainty in the detection. This is in agreement with the production of Fock states from mechanisms such as the joint emission of N atoms from an excited state [22]. One could establish this fact on firmer theoretical grounds by studying the indistinguishability of two bundles emitted by the system or of a bundle with an exact Fock state, by computing HOM interferences between the two arms of a beam-splitter. Such analyses have been conducted only recently in a dynamical setting [23] and their extension to characterize the output of an emitter, such as our N–photon source, will be presented in a future publication.

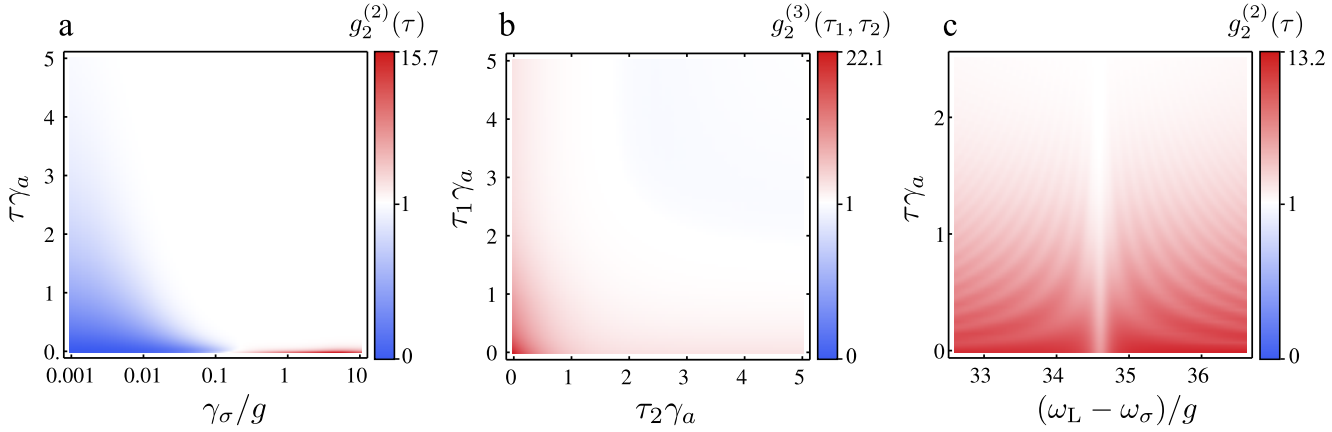

FIG. S6: **a**, Second order bundle correlation function $g_2^{(2)}(\tau)$ as a function of the QE decay rate γ_σ, showing how the emitter covers various regimes from antibunching of two-photon emission for lower γ_σ to bunching of two-photon emission for larger γ_σ, passing by coherent emission, $g_2^{(2)}(\tau)=1$ at intermediate $\gamma_\sigma\approx 0.2g$. Figures 3(h–i) in the text correspond to two vertical cuts at $\gamma_\sigma/g=0.01$ and $\gamma_\sigma/g=0.2$ of this figure. **b**, Third order bundle correlation function $g_2^{(3)}(\tau_1,\tau_2)$ at $\gamma_\sigma/g=0.2$. The correlation is unity except in a small window at small τ's due to the cavity jiter, supporting that the bundle emission is coherent to all orders. **c**, Bundle emission is coherent only when hitting the resonance, at $\omega_L\approx\omega_a+34.6g$, and displays a given, but no particular in any sense, dynamics out of resonance.

Finally, we have addressed before the question of the quantum state of one bundle. One could also pose the problem of the quantum state of the stream of the emission, which is however even more involved as it requires to describe the quantum state of the output field itself and therefore a non-trivial extension of the model. One can think, for instance, to study the quantum state of a quantum oscillator initially at rest, after its excitation for a given time by the emitter in the regime of N-photon emission. It is expected to produce a coherent superposition of multiples of N photons, that is to say, a brand of squeezing. All these questions are relevant for quantum applications and remain to be fully explored.

V. HIGHER ORDER N-PHOTON CORRELATIONS.

In the main text, we have established that the proposed emitter substitutes the basic unit of excitation of the light field—the photon—by the bundle (a packet of N photons), and that the conventional tools of quantum optics have to be upgraded consequently. Namely, the standard photon statistics when the system is in a regime of N-photon emission provides no particular result, while the bundle-statistics behaves in a meaningful way. We have stated that the bundle statistics can be tuned with the QE lifetime $1/\gamma_\sigma$. This is substantiated with Fig. S6a, that shows how $g_2^{(2)}(\tau)$ evolves from antibunched when γ_σ is small to bunched when it is large, passing by the regime of coherent emission in between, with $g_2^{(2)}(\tau)=1$. In the later case, the bundles are randomly distributed, which means that the emitter is coherent, in the sense of Glauber who understood that quantum optical coherence is linked to the statistics of the quanta, rather than to monochromaticity. This criterion is now commonly accepted to define lasing, for instance, the "atom laser" refers to a coherent matter wave, not to stimulated emission. To rigorously qualify our source as a laser of N-photon states, we have to show that the bundles are Poisson distributed not only at the level of pairs of bundles, i.e., that $g_2^{(2)}(\tau)=1$ as was shown in the text, but to all orders. This is shown in Fig. S6b with $g_2^{(3)}(\tau_1,\tau_2)$ that is seen to be close to 1, except in the jitter window (at small τ's), where the bundle can be resolved into its underlying photons. Since $g^{(n)}$ magnifies correlations as n increases, the approximation to a white square (corresponding to an ideal coherent signal) is actually excellent. Outside of the resonance, when the system does not behave as a N-photon emitter, the generalized correlation functions $g_N^{(n)}$ show no particular feature. This is illustrated in Fig. S6c for the case of lasing, where the sharp vertical line at $(\omega_L-\omega_a)/g\approx 34.6$ shows coherent bundle emission when hitting the resonance. The second order correlation function of the cavity field is not equal to one in the regime of coherent bundle emission (Fig. 4h of the text), so the cavity emission is not coherent if counting photons one by one. It becomes so at the N-photon level.

VI. EFFECT OF DECOHERENCE.

We have presented the scheme so far in an ideal system that suffers from no source of noise or decoherence apart from decay. It is one of the challenges of technology to keep these under control or remove them altogether to achieve any working quantum technology. It is still useful, however, to judge the present day feasi-

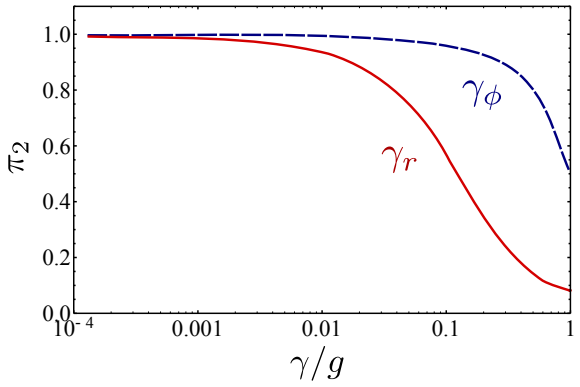

FIG. S7: (Colour online) Effect of the principal sources of noise in a semiconductor platform on the purity of two-photon emission in the regime where it is optimum. Rates of pure dephasing γ_ϕ (dashed blue) and cavity feeding at positive detuning γ_r (solid red) are varied independently up to the Rabi rate g of resonant exchange between the dot and the cavity. The mechanism is very robust against the generic source of decoherence that is pure dephasing γ_ϕ and is more sensible to cavity feeding γ_r. Values from the literature show that one can expect extremely performing N–photon emitters already with currently available samples.

bility of the proposed device by considering the impact of noise on its efficiency. We study in this Section the effect of both a generic source of decoherence, pure dephasing [8, 24], and of a particular source that is specific to semiconductor cavity QED in the configuration of our study, namely, cavity feeding [7, 25–28]. The former washes out the quantum coherence that links pure states, leading to a mixed density matrix. It is caused by a variety of detrimental agents, such as weak coupling to external baths, interactions, etc., and could be present to some extent in all experiments regardless of their implementation. The latter, cavity feeding, is proper to semiconductors and can be important even with a large detuning between the QE and the cavity. It is caused by the phonon-mediated transfer of an excitation between the QE—in this case, a quantum dot—and the cavity. The transfer can be predominant either from the QE to the cavity or the other way around depending on the detuning. The configuration of negative detuning Δ, when the dot is blue-detuned as compared to the cavity, is particularly harmful to the mechanism, since this is the one that transfers mainly towards the cavity due to an unavoidable spontaneous emission, therefore spoiling it with uncorrelated events. The reversed process, that transfers towards the dot, is assisted by the population of phonons available at the transition frequency $n_{\rm ph}(\Delta) = 1/(e^{\Delta/[k_{\rm B}T]} - 1)$ with no spontaneous emission term, and can thus be made small by lowering the temperature T. On the other hand, with negative detuning, the importance of these processes is reversed. As the scheme presented in the text is otherwise symmetric with respect to detuning, we will consider only the favourable red-detuned configuration. The model is extended to include these sources of decoherence and dephasing by adding to the master equation the three terms of the second line [7]:

$$\dot\rho = -i\,[H,\rho] + \Big[\frac{\gamma_a}{2}\mathcal{L}_a + \frac{\gamma_\sigma}{2}\mathcal{L}_\sigma + \frac{\gamma_\phi}{2}\mathcal{L}_{\sigma^\dagger\sigma} + \frac{(1+n_{\rm ph})\gamma_r}{2}\mathcal{L}_{\sigma^\dagger a} + \frac{n_{\rm ph}\gamma_r}{2}\mathcal{L}_{a^\dagger\sigma}\Big]\rho\,, \quad (11)$$

which are, like the decay terms, in the Lindblad form (Methods). The rate γ_ϕ accounts for the pure dephasing of the QE, while γ_r accounts for the phonon mediated coupling between the QD and the cavity. The case written is for negative detuning; the positive detuning counterpart exchanges the prefactors of the terms $\mathcal{L}(\sigma^\dagger a)$ and $\mathcal{L}(a^\dagger\sigma)$. The same procedure and analysis as detailed in the text can be carried out in the presence of these terms. We have considered them both independently in the regime of two-photon emission for the parameters of the text. The results are condensed in Fig. S7. Note that we did not look for the maximum purity of two-photon emission but considered how the optimum case without dephasing is affected by these two sources of decoherence. It is conceivable that the new terms are less harmful in other regimes (say at lower pumping) and that higher purities could be achieved in their presence. The figure shows that while decoherence does affect the purity of emission, the mechanism exhibits some robustness, with extended plateaus that set a goal for an optimum technology, while a fundamental demonstration appears within reach even in extremely noisy samples.

There is a clear physical reason why the mechanism is so resistant to dephasing. The main attribute to preserve is the bundle itself, that is to say, what is crucial is to maintain the ability of the system to release its energy exclusively in multiples of N. Now, the bundle emission takes place in a very small time window, that can be disrupted only for extremely large dephasing rates. The effect of dephasing for the rest of the time can have detrimental effects on other attributes such as the intensity of emission, but this is of little or no incidence for the usefulness of the device. This is the case for cavity feeding in the red-detuned configuration, where the transfer towards the dot can reduce the intensity of emission by blocking the QD. The excited QD releases its energy in a different solid angle and at a different frequency than the N-photon emission channel, so its spurious excitation is not damaging. As for the possibility to destroy a bundle by diverting one of its photons towards the QD rather than through the useful channel, since this is possible within the short time-window of emission only, this affects very little the purity. The scheme is even more resilient to pure dephasing, which is the most universal type of decoherence that one can expect to find in any system. The physical reason is also linked to the mechanism of bundles production, and is even less deleterious because it harms the QE alone with no concomitant penalty to the cavity. For most of the time, the QE undergoes Rabi oscillations driven by the laser. Their dephasing

is a cause of impediment for the buildup of the probability to have two photons, but this merely slows down the repetition rate. Once the state collapses, the whole cascade of photon emission unravels in the short time window, essentially shielded from dephasing of the QE. As a result, even with a considerable dephasing rate equal to the Rabi coupling rate, the mechanism still produces over 50% of two-photon bundles.

Now, in order to contrast Fig. S7 with the experimental state of the art: the semiconductor cavity QED literature reports largely varying values of dephasing rates, indicating that much room exists for optimization of the samples and reducing the sources of noise. Pure dephasing rates of $\gamma_\phi/g = 0.3$ have been estimated in the strong-coupling of a quantum dot to a microcavity at low temperature [24], and values as low as $\gamma_\phi/g = 0.025$ have been reported a few years later in similar semiconductor systems [7], with also a cavity feeding estimated at $\gamma_r/g = 0.025$. This shows that even the most noisy environment should already provide close to ideal two-photon emission. In atomic platforms, dephasing is so small that it is often neglected to fit the experimental results [29]. As for circuit QED, it has already reached the stage where dephasing is utterly negligible [30].

References

[1] Pearle, F. Wavefunction collapse and conservation laws. *Found. Phys.* **30**, 1145 (2000).

[2] Silverman, M. P. *Quantum superposition: counterintuitive consequences of coherence, entanglement, and interference* (Springer, 2008).

[3] Varcoe, B. T., Brattke, S., Weidinger, M. & Walther, H. Preparing pure photon number states of the radiation field. *Nature* **403** (2000).

[4] del Valle, E. Distilling one, two and entangled pairs of photons from a quantum dot with cavity QED effects and spectral filtering. *New J. Phys.* **15**, 025019 (2013).

[5] Greentree, A. D., Koch, J. & Larson, J. Fifty years of Jaynes–Cummings physics. *J. Phys. B: At. Mol. Opt. Phys.* **46**, 220201 (2013).

[6] Gies, C., Florian, M., Gartner, P. & Jahnke, F. The single quantum dot-laser: lasing and strong coupling in the high-excitation regime. *Opt. Express* **19**, 14370 (2011).

[7] Majumdar, A., Kim, E. D., Gong, Y., Bajcsy, M. & Vuckovic, J. Phonon mediated off-resonant quantum dot–cavity coupling under resonant excitation of the quantum dot. *Phys. Rev. B* **84**, 085309 (2011).

[8] Gonzalez-Tudela, A. *et al.* Effect of pure dephasing on the Jaynes-Cummings nonlinearities. *Opt. Express* **18**, 7002 (2010).

[9] Allen, L. & Eberly, J. H. *Optical Resonance and Two-Level Atoms* (Dover, 1987).

[10] Niemczyk, T. *et al.* Circuit quantum electrodynamics in the ultrastrong-coupling regime. *Nature Phys.* **6**, 772 (2010).

[11] Beaudoin, F., Gambetta, J. M. & Blais, A. Dissipation and ultrastrong coupling in circuit QED. *Phys. Rev. A* **84**, 043832 (2011).

[12] Forn-Díaz, P. *et al.* Observation of the Bloch-Siegert shift in a qubit-oscillator system in the ultrastrong coupling regime. *Phys. Rev. Lett.* **105**, 237001 (2010).

[13] Berlín, G. & Aliaga, J. Validity of the rotating wave approximation in the driven Jaynes–Cummings model. *J. Opt. B* **6**, 231 (2004).

[14] Hausinger, J. & Grifoni, M. Qubit-oscillator system under ultrastrong coupling and extreme driving. *Phys. Rev. A* **83**, 030301(R) (2011).

[15] Wallraff, A. *et al.* Strong coupling of a single photon to a superconducting qubit using circuit quantum electrodynamics. *Nature* **431**, 162 (2004).

[16] Fink, J. M. *et al.* Climbing the Jaynes–Cummings ladder and observing its $\sqrt{n}$ nonlinearity in a cavity QED system. *Nature* **454**, 315 (2008).

[17] Khitrova, G., Gibbs, H. M., Kira, M., Koch, S. W. & Scherer, A. Vacuum Rabi splitting in semiconductors. *Nat. Phys.* **2**, 81 (2006).

[18] Miller, R. *et al.* Trapped atoms in cavity QED: coupling quantized light and matter. *J. Phys. B.: At. Mol. Phys.* **38**, S551 (2005).

[19] Ridolfo, A., Leib, M., Savasta, S. & Hartmann, M. J. Photon blockade in the ultrastrong coupling regime. *Phys. Rev. Lett.* **109**, 193602 (2012).

[20] Bamba, M. & Ogawa, T. System-environment coupling derived by Maxwell's boundary conditions from the weak to the ultrastrong light-matter-coupling regime. *Phys. Rev. A* **88**, 013814 (2013).

[21] Schleich, P. *Quantum optics in phase space* (Wiley, 2011).

[22] Brown, K. R., Dani, K. M., Stamper-Kurn, D. M. & Whaley, K. B. Deterministic optical Fock-state generation. *Phys. Rev. B* **67**, 043818 (2003).

[23] Woolley, M. J., Lang, C., Eichler, C., Wallraff, A. & Blais, A. Signatures of Hong-Ou-Mandel interference at microwave frequencies. *New J. Phys.* **15**, 105025 (2013).

[24] Laucht, A. *et al.* Electrical control of spontaneous emission and strong coupling for a single quantum dot. *New J. Phys.* **11**, 023034 (2009).

[25] Hohenester, U. Cavity quantum electrodynamics with semiconductor quantum dots: Role of phonon-assisted cavity feeding. *Phys. Rev. B* **81**, 155303 (2010).

[26] Roy, C. & Hughes, S. Influence of electron–acoustic-phonon scattering on intensity power broadening in a coherently driven quantum-dot–cavity system. *Phys. Rev. X* **1**, 021009 (2011).

[27] Maragkou, M. *et al.* Bichromatic dressing of a quantum dot detected by a remote second quantum dot. *Phys. Rev. B* **88**, 075309 (2013).

[28] Florian, M., Gartner, P., Gies, C. & Jahnke, F. Phonon-mediated off-resonant coupling effects in semiconductor quantum-dot lasers. *New J. Phys.* **15**, 035019 (2013).

[29] Boca, A. *et al.* Observation of the vacuum Rabi spectrum for one trapped atom. *Phys. Rev. Lett.* **93**, 233603 (2004).

[30] Lang, C. *et al.* Correlations, indistinguishability and entanglement in Hong-Ou-Mandel experiments at microwave frequencies. *Nat. Phys.* **9**, 345 (2013).